Eur Biophys J (2002) 31: 172–178
DOI 10.1007/s00249-001-0197-8

ARTICLE

Simon Scheuring · Daniel J. Müller · Henning Stahlberg
Hans-Andreas Engel · Andreas Engel

# Sampling the conformational space of membrane protein surfaces with the AFM

Received: 10 August 2001 / Revised: 26 September 2001 / Accepted: 26 September 2001 / Published online: 29 January 2002


**Abstract** The atomic force microscope acquires topographs of single native membrane proteins at subnanometer resolution. Owing to the high signal-to-noise ratio, such images allow the conformational space of membrane protein surfaces to be sampled. This is demonstrated by topographs of porin OmpF, aquaporin-Z, and bacteriorhodopsin, all recorded at a lateral resolution of $<7$ Å and a vertical resolution of $\sim 1$ Å. The amplitudes of the domain movements were estimated from a large number of single molecule topographs and the corresponding energy landscapes calculated. To visualize the motion of protein domains, movies were generated by similarity ranking of the observed protein configurations. Electronic supplementary material to this paper can be obtained by using the Springer Link server located at http://dx.doi.org/10.1007/s00249-001-0197-8.

**Keywords** Loops · $\beta$-Turns · Membrane protein · Two-dimensional crystal · Energy landscape

Electronic supplementary material to this paper can be obtained by using the Springer Link server located at http://dx.doi.org/10.1007/s00249-001-0197-8

S. Scheuring · D.J. Müller · H. Stahlberg · A. Engel (✉)
M.E. Müller Institute for Microscopy at the Biozentrum,
University of Basel, Klingelbergstrasse 70,
4056 Basel, Switzerland
E-mail: andreas.engel@unibas.ch
Tel.: +41-61-2672261
Fax: +41-61-2672109

D.J. Müller
Max-Planck-Institute of Molecular Cell Biology and Genetics,
01307 Dresden, Germany

H.-A. Engel
Department of Physics and Astronomy,
University of Basel, Klingelbergstrasse 82,
4056 Basel, Switzerland

**Abbreviations** *AFM*: atomic force microscopy · *AqpZ*: aquaporin-Z · *bR*: bacteriorhodopsin · *EM*: electron microscopy · *FWHM*: full width half maximum · *OmpF*: outer membrane protein F · *SD*: standard deviation

## Introduction

The atomic force microscope (AFM) (Binnig et al. 1986) allows surface topographs of protein complexes to be acquired under native conditions at a resolution of 5–10 Å (Schabert et al. 1995; Mou et al. 1996; Miles 1997; Czajkowsky and Shao 1998; Scheuring et al. 1999; Seelert et al. 2000). In order to achieve high resolution, the pH and ionic strength of the buffer solution should be adjusted to balance the van der Waals and electrostatic interactions between the tip and sample, resulting in net sample loading forces of 100 pN (Müller et al. 1999b). The quality of such topographs has been assessed by comparison with 3D structures from X-ray and electron crystallography (Karrasch et al. 1994; Schabert et al. 1995; Müller and Engel 1999; Müller et al. 2000; Scheuring et al. 2000). Accordingly, the AFM allows polypeptide loops connecting transmembrane $\alpha$-helices or antiparallel $\beta$-strands of membrane proteins to be identified (Scheuring et al. 1999; Müller et al. 2000).

To corroborate loop assignments, the volume of surface protruding structures can be compared to topology predictions (Scheuring et al. 1999, 2001). Owing to the high signal-to-noise ratio of topographs, the stoichiometry of oligomeric complexes can be determined from unprocessed images (Mou et al. 1995; Reviakine et al. 1998; Czajkowsky et al. 1999; Seelert et al. 2000; Scheuring et al. 2001; Stahlberg et al. 2001) and defects of individual molecules visualized (Müller et al. 1999a).

Here we examine large numbers of topographs of individual membrane protein oligomers recorded with an AFM under physiological conditions [outer membrane protein F (OmpF); aquaporin-Z (AqpZ); bacteriorhodopsin (bR) ($\sim$200 pN and $\sim$100 pN)]. Standard image processing algorithms demonstrate that these

topographs contain surface contour information at a lateral resolution of $< 7$ Å and a vertical resolution of $\sim 1$ Å. The positions of surface protruding domains of each particle were determined; from the resulting position, probability maps and energy landscapes were calculated. Finally, the particles were aligned and ordered by their similarity and merged into movies (http://www.mih.unibas.ch/movies.html). Since the number of surface features is low ($\sim 10$) and the number of individual images high, the smoothly moving movies represent a random walk through the possible surface conformations and thereby a sampling of the surface conformation energy landscape.

## Materials and methods

### Sample preparation

2D crystals of AqpZ and OmpF were grown by dialysis of protein-lipid-detergent mixtures (Hoenger et al. 1990; Ringler et al. 1999). Before AFM imaging, samples were checked by negative stain electron microscopy for their crystallinity and by gel electrophoresis for their purity. Purple membranes were prepared as described (Oesterhelt and Stoeckenius 1974).

### Atomic force microscopy

Mica prepared as described (Schabert and Engel 1994) was used as support. High-resolution topographs were acquired in buffer solution (Müller and Engel 1999; Müller et al. 1999c; Scheuring et al. 1999), where the pH and ionic strength of the recording buffers were adjusted to achieve high resolution (Müller et al. 1999b). All buffers were prepared using nanopure water (18 MW/cm) and analytical grade chemicals. Imaging was performed with a commercial Nanoscope III AFM (Digital Instruments, Santa Barbara, Calif., USA) equipped with a 120 μm scanner (J-scanner) and oxide-sharpened pyramidal $Si_3N_4$ tips mounted on triangular 100-μm-long cantilevers ($k = 0.09$ N/m) (Olympus, Tokyo, Japan). The AFM was operated in contact mode applying minimal forces (100 pN, unless specified) at a scan frequency of 4–6 Hz. The pixel size was 2.4–3.4 Å.

### Image processing

Topographs of individual proteins were aligned using the SEMPER image processing system (Saxton et al. 1979). To assess the resolution, phase residuals and spectral signal-to-noise (Unser et al. 1987) were calculated by comparing two independent averages from aligned single molecule images.

The position $r$ of each protrusion peak was determined within a search radius equal to the resolution limit. We have then extracted the probability distributions $p_d(r)$ that the protrusion peak of domain $d$ is at position $r$. Because of the thermal motion of the domains, each domain configuration with energy $E$ is realized with a probability proportional to the Boltzmann factor. However, there might be several domain configurations that have a protrusion peak at the same position. Then, the probability distribution $p_d(r)$ is proportional to the partition function $Z(r) = \sum \exp\{-E/kT\}$, where the sum is taken over all domain configurations with peak position $r$ (note that we take $r$ as a thermodynamic parameter). Thus, the (effective) free energy can be calculated by $F_d = -kT \ln p_d(r)$, which represents the energy landscape within which the domains are moving. Here, we have assumed that the probability distributions $p_d$ of different domains are uncorrelated, i.e., that the individual loops move independently from each other.

To generate the protein motion movie, the average image was used as a first reference (and first frame in the movie) and cross-correlated with all particles. The particle image with the highest cross-correlation value was labeled particle 1 (second frame in the movie), and was used as the new reference to select particle 2 (third frame in the movie) which shows the highest similarity to particle 1 from the rest of the molecules. This was repeated to similarity rank all particle images to produce Quicktime movies using QuicktimePro (http://www.quicktime.com). We have analyzed the positions within the similarity ranking of the same particle in subsequent AFM scans, recorded in time steps of 1.5 min. The average distance and its standard deviation (SD) of the particle positions indicate a random distribution. Thus, there is no time-correlation of the domain configurations in subsequent scans, i.e., the protein motion cannot be resolved. However, this limitation is overcome by reconstructing a motion sequence by similarity ranking.

All images displayed were rendered as 15° tilted surface representations using the Image SXM program (Steve Barrett, http://reg.ssci.liv.ac.uk/).

## Results and discussion

Highly ordered 2D crystals of OmpF, AqpZ, and bR were firmly attached to atomically flat mica surfaces through physisorption (Müller et al. 1995b; Schabert et al. 1995; Müller and Engel 1999; Scheuring et al. 1999). After adsorption, the forces between the biological membranes and the AFM tip were electrostatically balanced by adjustment of pH and ionic strength of the buffer solution to achieve minimal sample loading (Müller and Engel 1999; Müller et al. 1999c; Scheuring et al. 1999).

The topograph quality was assessed by calculating the phase residual and the spectral signal-to-noise ratio (Schabert and Engel 1994). Unprocessed topographs recorded from OmpF, AqpZ, and bR (Figs. 1a, 2a, 3a, b) are essentially "noise-free", and thus allow features of individual particles to be resolved to better than 7 Å lateral resolution, as indicated by different resolution criteria (Figs. 1b, c, 2b, c, 3c, d). From such AFM images, typically 1500 high-resolution topographs of single oligomers were extracted, aligned, and ordered (see Materials and methods). We have analyzed these topographs by calculating averages, SD maps, and by developing and applying two new methods. Firstly, we extract the probability distribution of the protrusion peaks. This allows us to gain further statistical information about the domain configuration, which is not accessible in SD maps. Further, the thermal motion of the protein probes its configuration space which allows the free energy landscape of the domains to be extracted. Secondly, we reconstruct the motion of the proteins by similarity ranking of individual configurations. Analysis of time sequences resulting from multiple scans of identical areas demonstrates that identical particles are randomly positioned in similarity ranked particle sequences. Hence, by similarity ranking of large numbers of particles we can reconstruct protein dynamics that are faster than the time resolution obtained by subsequent AFM scans.

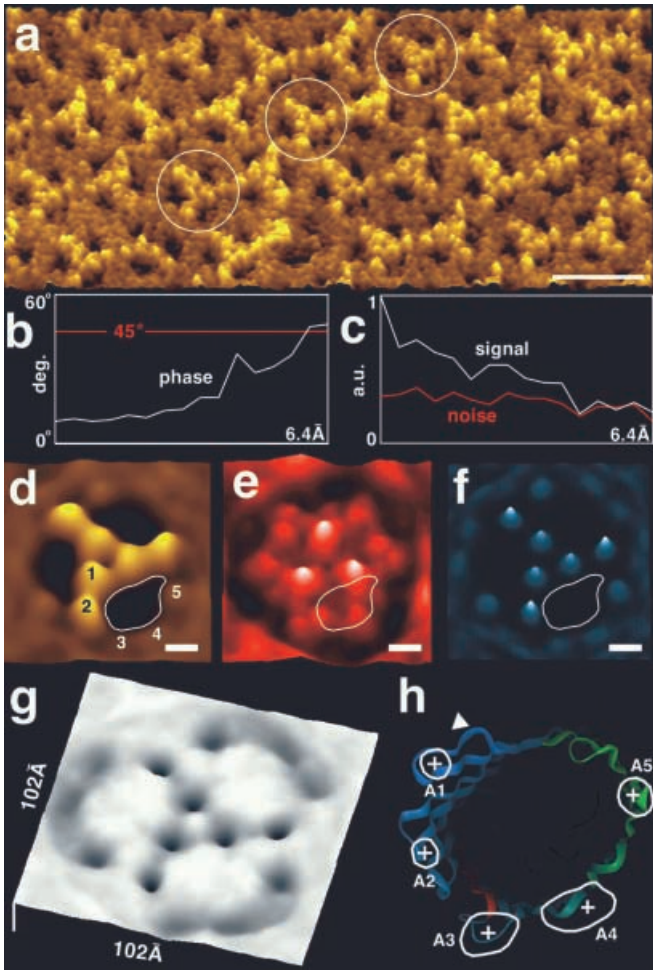


**Fig. 1** **a** High-resolution raw data AFM image of an OmpF 2D crystal exposing the periplasmic surface to the tip imaged with a loading force to the tip of ~100 pN. *Circles* indicate individual protein surfaces (*scale bar*: 10 nm; full gray scale: 10 Å). **b** Phase residual analysis from averaging 1477 topographs of the OmpF periplasmic surface. The Nyquist frequency is 1/(6.4 Å). **c** Spectral signal-to-noise ratio analysis from averaging the 1477 OmpF topographs. The Nyquist frequency is 1/(6.4 Å). **d** Average topograph calculated from a total of 1477 aligned trimers. Detectable protrusions are numbered (compare with **h**); the pore is outlined (*scale bar*: 10 Å). **e** Standard deviation map corresponding to average **d**. The pore position is outlined (*scale bar*: 10 Å; full gray scale range: 0.1–0.5 Å). **f** Position probability map calculated from the peak position distribution of 1477 aligned trimers (see Materials and methods). The pore position is outlined (*scale bar*: 10 Å). **g** Energy landscape as function of protrusion peak position (full image size: 102 Å; $\Delta kT = 5.0$). **h** Overlay of the FWHM outline to a monomer of the porin OmpF atomic model (Cowan et al. 1992). The *crosses* indicate the top probability positions. The *triangle* outside the monomer indicates the three-fold axis symmetry center

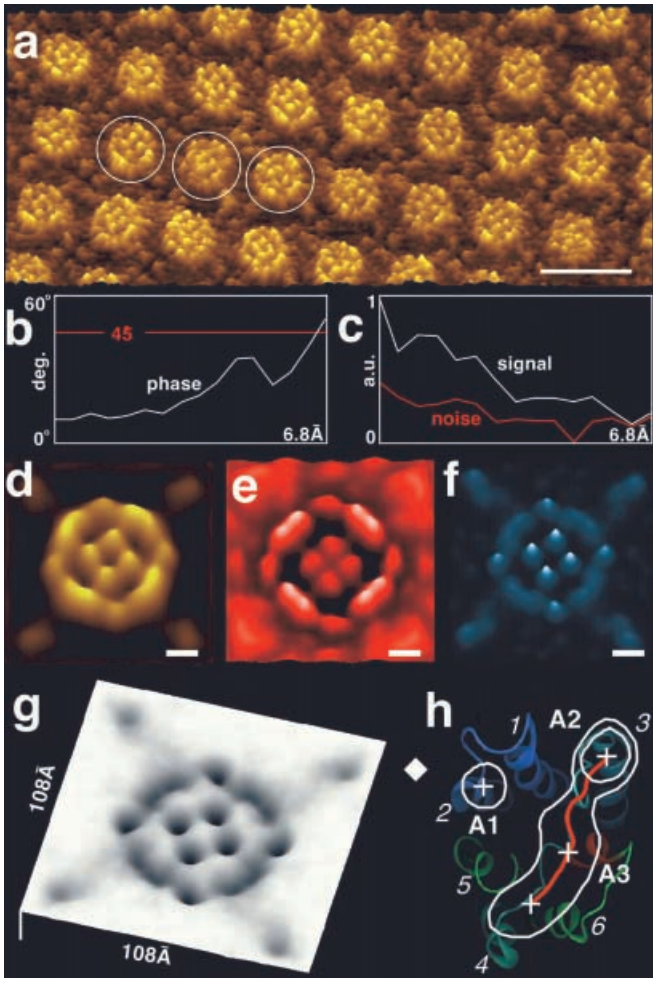


**Fig. 2** **a** High-resolution raw data AFM image of an AqpZ 2D crystal. *Circles* indicate individual extracellular protein surfaces imaged at a loading force to the tip of ~80 pN (*scale bar*: 100 Å; full gray scale: 10 Å). **b** Phase residual analysis from averaging 1447 topographs of the AqpZ extracellular surface. The Nyquist frequency is 1/(6.8 Å). **c** Spectral signal-to-noise ratio analysis from averaging the 1447 AqpZ topographs. The Nyquist frequency is 1/(6.8 Å). **d** Average topograph calculated from a total of 1447 aligned tetramers (*scale bar*: 10 Å; full gray scale range: 0.1–0.7 Å). **e** Standard deviation map corresponding to average **d** (*scale bar*: 10 Å). **f** Position probability map calculated from the peak position distribution of 1447 aligned tetramers (see Materials and methods) (*scale bar*: 10 Å). **g** Energy landscape as function of protrusion peak position (full image size: 108 Å; $\Delta kT = 6.6$). **h** Overlay of the FWHM outline and a model of the AQP1 structure (Murata et al. 2000). The *crosses* indicate the highest probability positions, the *red line* the top probability tracing line of loop C. Transmembrane helices are numbered in *italics* (helices *1* and *2* connected by loop A (FWHM: A1); helices *3* and *4* connected by loop C (FWHM: A3); the end of helix 3 protrudes from membrane surface, yielding the stable domain delineated by contour A2; helices *5* and *6* are connected by loop E which folds back into the water channel). The *diamond* outside the monomer indicates the four-fold axis symmetry center

## Analysis of the OmpF surface

OmpF is a $\beta$-barrel protein that forms stable trimers (Cowan et al. 1992). High-resolution topographs of 2D crystals (Fig. 1a) reveal details of the periplasmic OmpF surface at 6.6 Å resolution (Fig. 1b, c). The $\beta$-turns connecting the $\beta$-strands can be distinguished on the averaged AFM topograph from 1477 particles of the periplasmic surface (Fig. 1d) (Müller and Engel 1999). Two strongly protruding $\beta$-turns are seen close to the three-fold symmetry center of each monomer (“1” and “2” in Fig. 1d). The three peripheral protrusions 3–5

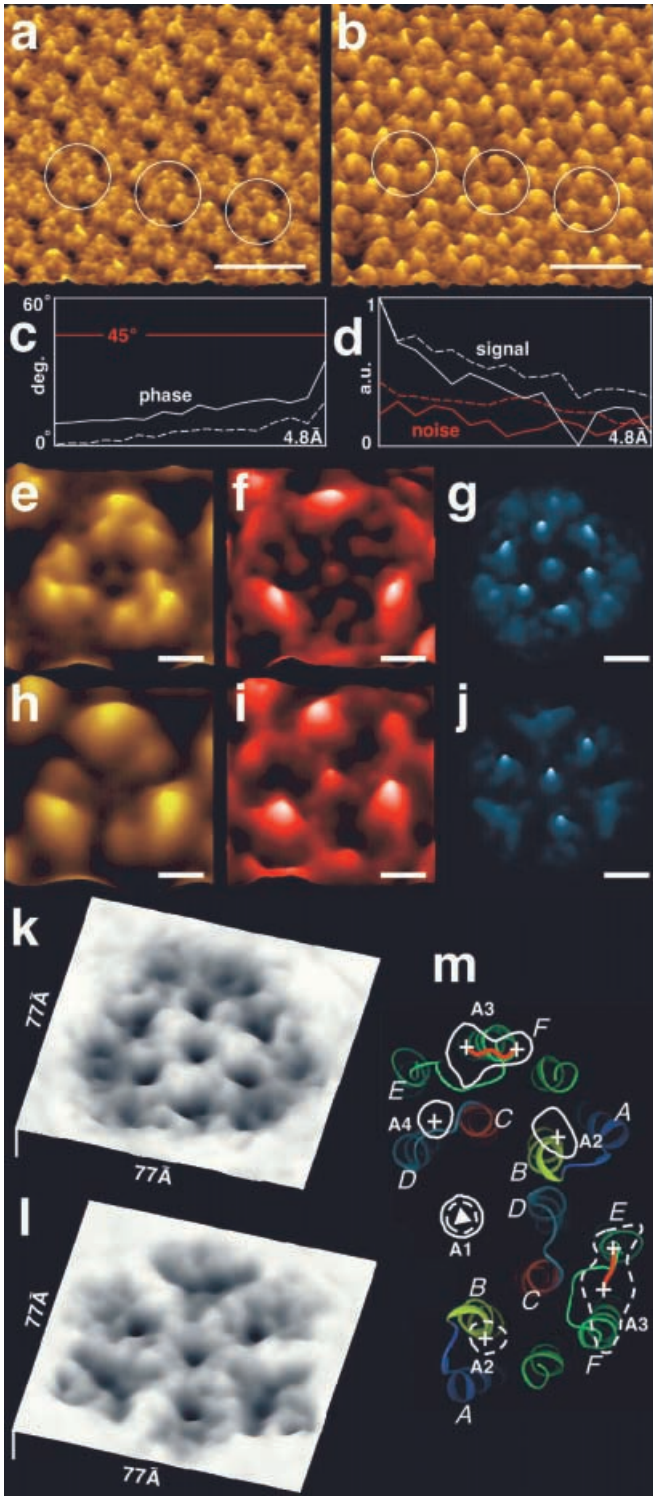


**Fig. 3** **a** High-resolution raw data AFM topograph of a bR 2D crystal exposing the cytoplasmic surface. *Circles* indicate individual protein surfaces imaged at a loading force to the tip of ~200 pN; **b** AFM topograph of a bR 2D crystal exposing the cytoplasmic surface imaged at a loading force to the tip of ~100 pN (*scale bars*: 10 nm; full gray scale: 10 Å). **c** Phase residual analysis from averaging 800 topographs of the cytoplasmic bR surface recorded with ~200 pN (*continuous line*), and 1403 topographs recorded with ~100 pN loading force applied to the tip (*dashed line*). The Nyquist frequency is 1/(4.8 Å). **d** Spectral signal-to-noise ratio analysis from averaging the 800 bR topographs recorded with ~200 pN (*continuous lines*), and the 1403 bR topographs recorded with ~100 pN loading force applied to the tip (*dashed lines*). The Nyquist frequency is 1/(4.8 Å). **e** Average topograph calculated from a total of 800 trimers recorded with ~200 pN loading force applied to the tip (*scale bar*: 10 Å). **f** Standard deviation map corresponding to average **e** (*scale bar*: 10 Å; full gray scale range: 0.1–0.3 Å). **g** Position probability map calculated from the peak position distribution of 800 aligned trimers recorded with ~200 pN loading force applied to the tip (see Materials and methods) (*scale bar*: 10 Å). **h** Average topograph calculated from a total of 1403 aligned trimers recorded with ~100 pN loading force applied to the tip (*scale bar*: 10 Å). **i** Standard deviation map corresponding to average **h** (*scale bar*: 10 Å; full gray scale range: 0.1–0.5 Å). **j** Position probability map obtained by making a peak search on the 1403 aligned trimers recorded with ~100 pN loading force applied to the tip (see Materials and methods) (*scale bar*: 10 Å). **k** Energy landscape as a function of protrusion peak position (full image size: 77 Å; $\Delta kT = 5.7$); determined from 800 topographs recorded at ~200 pN. **l** Energy landscape as a function of protrusion peak position (full image size: 77 Å; $\Delta kT = 4.5$); determined from the 1403 topographs recorded at ~100 pN. **m** Overlay of the FWHM outline, derived from the topographs acquired with ~200 pN (*continuous line*) and with ~100 pN (*dashed line*) loading force applied to the tip, and two monomers of the bR atomic model (Mitsuoka et al. 1999). The *crosses* indicate the highest probability positions. Transmembrane helices are numbered in *italics* [helices A and B connected by the A-B loop (FWHM: A2); helices C and D connected by the C-D loop (FWHM: A4); helices E and F connected by the E-F loop (FWHM: A3)]. The *triangle* labeled A1 outside the monomer indicates the three-fold axis symmetry center

correlate with two $\beta$-turns ("A4" and "A5") and one loop ("A3") displayed in Fig. 1h. The corresponding SD map (Fig. 1e) shows one strong signal ($\pm 0.7$ Å) on the edge of $\beta$-turn "1" towards the channel cavity. A smaller deviation signal is detected in the channel, whereas the protein regions at the trimer periphery exhibit a SD of $\pm 0.1$ Å (Fig. 1e). The probability map (Fig. 1f) shows faint but sharp peaks, indicating that $\beta$-turns "1" and "2" are rather rigid structures with low flexibility and small lateral movement amplitudes. In agreement, the corresponding minima in the energy landscape (Fig. 1g) are of uniform narrow width, reflecting the rigid architecture of the $\beta$-barrel protein (Fig. 1h). The areas at full width half maximum (FWHM) of the peaks in the probability map correspond to 27 Å$^2$ and 23 Å$^2$ for the central $\beta$-turns (Fig. 1h, A1, A2). In contrast, the FWHM area is 78 Å$^2$ for the peripheral protrusion corresponding to the loop connection (Fig. 1h, A3), while the other two peripheral $\beta$-turns have areas of 98 Å$^2$ and 42 Å$^2$ at the FWHM (Fig. 1h, A4, A5). The movie generated from the 1477 individual aligned and ordered topographs shows relatively little movement of the surface protruding protein domains (Movie 1, OmpF; http://www.mih.unibas.ch/movies.html).

## Analysis of the AqpZ surface

No atomic level structure has so far been published for AqpZ. Ringler et al. (1999) have acquired a cryo-electron microscopy (EM) projection map from 2D AqpZ

crystals at 8 Å resolution. This map is similar to that obtained from AQP1 (Walz et al. 1995), for which an atomic model derived from EM data has been published (Murata et al. 2000). The similarity is in agreement with the high sequence homology found throughout the aquaporin family (Heymann and Engel 2000). Topographs recorded with the AFM have been used to identify the extracellular surface of AqpZ (Scheuring et al. 1999) (Fig. 2a). In addition, the polypeptide loops have been assigned based on the volume of protruding domains (Scheuring et al. 1999), subsequently confirmed by the position of the α-helices connected by them (Scheuring et al. 2000). The average calculated from 1447 topographs (Fig. 2d) features 12 protrusions per tetramer. On each monomer, one small protrusion is close to the tetramer center, while one small and one large elongated protrusion are on the periphery of the protein (Scheuring et al. 1999). The SD map (Fig. 2e) shows maximal signals on the large peripheral protrusion, which has been identified as the large C-loop connecting α-helices 3 and 4. Correspondingly, the position probability map (Fig. 2f) shows a broad distribution on loop C, while the other two protrusions result in sharp peaks. The sharp protrusion peak in the proximity of the four-fold symmetry axis has been assigned to loop A. The other peak corresponds to the end of helix 3 at the periphery (Scheuring et al. 1999, 2000). The energy landscape represents loop C as a shallow curved groove (Fig. 2g), indicating that loop C does not form a straight connection between helix 3 and 4 (Fig. 2g). In contrast, the energy minima of the other two domains are deeper and narrower. The overlay of the FWHM areas of 263 $Å^2$ (A3) of loop C and 33 $Å^2$ (A1) and 42 $Å^2$ (A2) of the small central and the small peripheral protrusions document very different movement amplitudes of the different membrane protruding domains (Fig. 2h). The 1447 topographs were similarity ranked to assemble a movie (Movie 2, AqpZ; http://www.mih.unibas.ch/movies.html). In agreement with the probability map (Fig. 2f), the movie reflects the high stability of the protrusions close to the four-fold symmetry center and the small peripheral protrusions, with both showing almost no movements. The peripheral C-loop [~26 amino acids (aa)], however, has a high positional freedom along the connection between helices 3 and 4, which is reflected by wave-like movements along this polypeptide stretch (Movie 2, AqpZ).

## Analysis of the bR surface

Bacteriorhodopsin is a light-driven proton pump comprising seven transmembrane helices. Its structure has been solved by both EM (Henderson and Unwin 1975; Mitsuoka et al. 1999) and X-ray crystallography (Pebay-Peyroula et al. 1997; Sass et al. 1997; Luecke et al. 1999). Helices E and F are connected by a long loop of 16 aa (Mitsuoka et al. 1999). By changing the force applied to the AFM tip during scanning, this long loop can be contoured in its extended conformation at minimal force (Fig. 3b, h) and can be pushed away while imaging at higher force (Fig. 3a, e and Müller et al. 1995a, 1999c). As a result, the loops connecting helices A and B, and C and D, are only contoured under high force conditions (~200 pN) (Fig. 3a, e). Under both recording conditions a faint protrusion in the trimer center is visible, which has been identified as a highly ordered lipid molecule (Müller et al. 1999c). The phase residual and spectral signal-to-noise ratio document a resolution extending to the Nyquist frequency of $(4.8 Å)^{-1}$ (Fig. 3c, d). The SD maps calculated from topographs of 1403 bR trimers acquired with ~100 pN (minimal) and of 800 bR trimers recorded with ~200 pN loading force reflect the high flexibility of the E-F loop on the periphery of the molecule (Fig. 3f, i). The position probability maps show a high positional preservation of the A-B loop and the central lipid molecule for both imaging conditions (Fig. 3g, j). Under minimal force imaging conditions, both the SD map and the position probability map show a signal in the trimer center (Fig. 3i, j). The signal in the SD map (Fig. 3i) indicates that the central lipid molecule cannot be detected in all particles. On the other hand, the position probability map demonstrates high positional conservation of this protrusion (Fig. 3j). Since the E-F loop in minimal force topographs is extended, the probability map only shows a broad distribution in the region of the E-F loop (Fig. 3j). This dominance of the E-F loop under low force imaging conditions also becomes apparent with its broad energy minimum in the energy landscape of bR (Fig. 3l). Thus the C-D loop can only be detected as a protrusion in the high force map (Fig. 3g), since it is covered by the E-F loop in minimal force topographs. Overlays of the top peak positions (indicated by crosses in Fig. 3m) and the FWHM areas (continuous line: ~200 pN; dashed line: ~100 pN) with two monomers of the atomic model [Fig. 3m (Mitsuoka et al. 1999)] illustrate the structural difference under the two imaging conditions. The overlay derived from the probability map calculated from the data acquired at ~200 pN reveals the central protrusion corresponding to a highly ordered lipid, FWHM area 26 $Å^2$ (A1), loop A-B, FWHM area 30 $Å^2$ (A2), loop E-F, FWHM area 90 $Å^2$ (A3), and loop C-D, FWHM area 19 $Å^2$ (A4). Under minimal force conditions (~100 pN) the first three loops reveal FWHM areas of 16 $Å^2$ (A1), 21 $Å^2$ (A2), and 121 $Å^2$ (A3); loop C-D cannot be detected when loop E-F is extended (compare Fig. 3g with j, and see Fig. 3m). At minimal forces, loop E-F reveals a strongly asymmetric position probability, distributed between helices E and F (Fig. 3m). At higher forces the corresponding FWHM area is mainly located on top of helix F that protrudes further out of the membrane than helix E (Fig. 3m). Movies were generated from 800 and 1403 topographs acquired at loading forces of ~200 pN and ~100 pN (Movie 3, $bR_{(200\ pN)}$; Movie 4, $bR_{(100\ pN)}$;

http://www.mih.unibas.ch/movies.html). The movie assembled from particles imaged at ~200 pN shows essentially little loop movements. The long loop E-F in its compressed state represents the most flexible part, in agreement with the surface probability map (Movie 3, $bR_{(200\ pN)}$; see also Fig. 3g). Similarity ranked images recorded at ~100 pN show loop E-F in the extended state, which is strongly flexible and shows wave-like movements (Movie 4, $bR_{(100\ pN)}$; see also Fig. 3j).

## Conclusions

Structural biological techniques, which require averaging processes to extract structure information, cannot assess the individuality and flexibility of proteins. Because biological processes are directly related to the flexibility of individual proteins, the assessment of flexibility information on a single molecule level is of major importance to detect structure-function relationships. As demonstrated here, the AFM can sample the conformational space of membrane protein surfaces at a lateral resolution reaching 5 Å and at a vertical resolution of 1 Å. We have developed and applied methods to interpret large numbers of single molecule images. These include calculating position probability maps of protruding domains and corresponding free energy landscapes. Further, we convert the random, time-unresolved sampling of the motion of the protruding domains into similarity ranked movie sequences. This approach promises a wide range of applications. Firstly, SD and position probability maps provide additional structural information on native protein surfaces, revealing the existence of rigid and flexible loops as well as their positions. Secondly, the surface motions of membrane proteins are likely to change profoundly upon ligand binding. Position density maps will therefore provide information on binding site and binding dynamics. Thirdly, signals to induce a biological process can be applied while scanning the sample with the AFM stylus. The subsequently similarity ranked single molecule images will provide a deep insight into the nanomechanics of the function-related conformational change. These possibilities will be enhanced by the improvements in sensitivity and speed of future atomic force microscopes (Viani et al. 1999).

**Acknowledgements** The authors would like to thank Drs. S.A. Müller and H. Grubmüller for critical comments on the manuscript. This work was supported by the Swiss National Foundation for Scientific Research (grant 3100-059415.99 to A.E.) and the Maurice E. Müller Foundation of Switzerland.

## References

Binnig G, Quate CF, Gerber C (1986) Atomic force microscope. Phys Rev Lett 56:930–933

Cowan SW, Schirmer T, Rummel G, Steiert M, Ghosh R, Pauptit RA, Jansonius JN, Rosenbusch JP (1992) Crystal structures explain functional properties of two *E. coli* porins. Nature 358:727–733

Czajkowsky DM, Shao Z (1998) Submolecular resolution of single macromolecules with atomic force microscopy. FEBS Lett 430:51–54

Czajkowsky DM, Iwamoto H, Cover TL, Shao Z (1999) The vacuolating toxin from *Helicobacter pylori* forms hexameric pores in lipid bilayers at low pH. Proc Natl Acad Sci USA 96:2001–2006

Henderson R, Unwin PNT (1975) Three-dimensional model of purple membrane obtained by electron microscopy. Nature 257:28–32

Heymann JB, Engel A (2000) Structural clues in the sequences of the aquaporins. J Mol Biol 295:1039–1053

Hoenger A, Gross H, Aebi U, Engel A (1990) Localization of the lipopolysaccharides in metal-shadowed reconstituted lipid-porin membranes. J Struct Biol 103:185–195

Karrasch S, Hegerl R, Hoh J, Baumeister W, Engel A (1994) Atomic force microscopy produces faithful high-resolution images of protein surfaces in an aqueous environment. Proc Natl Acad Sci USA 91:836–838

Luecke H, Schobert B, Richter HT, Cartailler JP, Lanyi JK (1999) Structure of bacteriorhodopsin at 1.55 Å resolution. J Mol Biol 291:899–911

Miles M (1997) Scanning probe microscopy: probing the future. Science 277:1845–1846

Mitsuoka K, Hirai T, Murata K, Miyazawa A, Kidera A, Kimura Y, Fujiyoshi Y (1999) The structure of bacteriorhodopsin at 3.0 Å resolution based on electron crystallography: implication of the charge distribution. J Mol Biol 286:861–882

Mou JX, Yang J, Shao ZF (1995) Atomic force microscopy of cholera toxin B-oligomers bound to bilayers of biologically relevant lipids. J Mol Biol 248:507–512

Mou J, Sheng S, Ho R, Shao Z (1996) Chaperonins GroEL and GroES: views from atomic force microscopy. Biophys J 71:2213–2221

Müller DJ, Engel A (1999) pH and voltage induced structural changes of porin OmpF explain channel closure. J Mol Biol 285:1347–1351

Müller DJ, Büldt G, Engel A (1995a) Force-induced conformational change of bacteriorhodopsin. J Mol Biol 249:239–243

Müller DJ, Schabert FA, Büldt G, Engel A (1995b) Imaging purple membranes in aqueous solutions at subnanometer resolution by atomic force microscopy. Biophys J 68:1681–1686

Müller DJ, Baumeister W, Engel A (1999a) Controlled unzipping of a bacterial surface layer with atomic force microscopy. Proc Natl Acad Sci USA 96:13170–13174

Müller DJ, Fotiadis D, Scheuring S, Müller SA, Engel A (1999b) Electrostatically balanced subnanometer imaging of biological specimens by atomic force microscopy. Biophys J 76:1101–1111

Müller DJ, Sass H-J, Müller S, Büldt G, Engel A (1999c) Surface structures of native bacteriorhodopsin depend on the molecular packing arrangement in the membrane. J Mol Biol 285:1903–1909

Müller DJ, Heymann JB, Oesterhelt F, Moller C, Gaub H, Büldt G, Engel A (2000) Atomic force microscopy of native purple membrane. Biochim Biophys Acta 1460:27–38

Murata K, Mitsuoka K, Hirai T, Walz T, Agre P, Heymann JB, Engel A, Fujiyoshi Y (2000) Structural determinants of water permeation through aquaporin-1. Nature 407:599–605

Oesterhelt D, Stoeckenius W (1974) Isolation of the cell membrane of *Halobacterium halobium* and its fraction into red and purple membrane. Methods Enzymol 31:667–678

Pebay-Peyroula E, Rummel G, Rosenbusch JP, Landau EM (1997) X-ray structure of bacteriorhodopsin at 2.5 angstroms from microcrystals grown in lipidic cubic phases. Science 277:1676–1681

Reviakine I, Bergsma-Schutter W, Brisson A (1998) Growth of protein 2-D crystals on supported planar lipid bilayers imaged in situ by AFM. J Struct Biol 121:356–361

Ringler P, Borgnia MJ, Stahlberg H, Maloney PC, Agre P, Engel A (1999) Structure of the water channel AqpZ from *Escherichia*

*coli* revealed by electron crystallography. J Mol Biol 291:1181–1190

Sass HJ, Schachowa IW, Rapp G, Koch MHJ, Oesterhelt D, Dencher NA, Büldt G (1997) The tertiary structural changes in bacteriorhodopsin occur between M states: X-ray diffraction and Fourier transform infrared spectroscopy. EMBO J 16:1484–1491

Saxton WO, Pitt TJ, Horner M (1979) Digital image processing: the semper system. Ultramicroscopy 4:343–354

Schabert FA, Engel A (1994) Reproducible acquisition of *Escherichia coli* porin surface topographs by atomic force microscopy. Biophys J 67:2394–2403

Schabert FA, Henn C, Engel A (1995) Native *Escherichia coli* OmpF porin surfaces probed by atomic force microscopy. Science 268:92–94

Scheuring S, Ringler P, Borgina M, Stahlberg H, Müller DJ, Agre P, Engel A (1999) High resolution topographs of the *Escherichia coli* waterchannel aquaporin Z. EMBO J 18:4981–4987

Scheuring S, Tittmann P, Stahlberg H, Ringler P, Borgina M, Agre P, Gross H, Engel A (2000) The aquaporin sidedness revisited. J Mol Biol 299:1271–1278

Scheuring S, Freiss-Husson F, Engel A, Rigaud J-L, Ranck J-L (2001) High resolution topographs of the *Rubrivivax gelatinosus* light-harvesting complex 2. EMBO J 20:3029–3035

Seelert H, Poetsch A, Dencher NA, Engel A, Stahlberg H, Müller DJ (2000) Proton powered turbine of a plant motor. Nature 405:418–419

Stahlberg H, Müller DJ, Suda K, Fotiadis D, Engel A, Matthey U, Meier T, Dimroth P (2001) Bacterial ATP synthase has an undecameric rotor. EMBO Rep 2:229–235

Unser M, Trus BL, Steven AC (1987) A new resolution criterion based on spectral signal-to-noise ratios. Ultramicroscopy 23:39–52

Viani MB, Schäfer TE, Chand A, Rief M, Gaub H, Hansma PK (1999) Small cantilevers for force spectroscopy of single molecules. J Appl Phys 86:2258–2262

Walz T, Typke D, Smith BL, Agre P, Engel A (1995) Projection map of aquaporin-1 determined by electron crystallography. Nat Struct Biol 2:730–732